

Dust to Tower: Coarse-to-Fine Photo-Realistic Scene Reconstruction from Sparse Uncalibrated Images

Xudong Cai¹ Yongcai Wang^{1*} Zhaoxin Fan^{2*} Deng Haoran¹ Shuo Wang¹
Wanting Li¹ Deying Li¹ Lun Luo³ Minhong Wang³ Jintao Xu³

¹School of Information, Renmin University of China, Beijing, China

²Beijing Advanced Innovation Center for Future Blockchain and Privacy Computing,
Institute of Artificial Intelligence, Beihang University, Beijing, China

³HAOMO.AI, Beijing, China

Abstract

Photo-realistic scene reconstruction from sparse-view, uncalibrated images is highly required in practice. Although some successes have been made, existing methods are either Sparse-View but require accurate camera parameters (i.e., intrinsic and extrinsic), or SfM-free but need densely captured images. To combine the advantages of both methods while addressing their respective weaknesses, we propose **Dust to Tower (D2T)**, an accurate and efficient coarse-to-fine framework to optimize 3DGS and image poses simultaneously from sparse and uncalibrated images. Our key idea is to first construct a coarse model efficiently and subsequently refine it using warped and inpainted images at novel viewpoints. To do this, we first introduce a Coarse Construction Module (CCM) which exploits a fast Multi-View Stereo model to initialize a 3D Gaussian Splatting (3DGS) and recover initial camera poses. To refine the 3D model at novel viewpoints, we propose a Confidence Aware Depth Alignment (CADA) module to refine the coarse depth maps by aligning their confident parts with estimated depths by a Mono-depth model. Then, a Warped Image-Guided Inpainting (WIGI) module is proposed to warp the training images to novel viewpoints by the refined depth maps, and inpainting is applied to fulfill the “holes” in the warped images caused by view-direction changes, providing high-quality supervision to further optimize the 3D model and the camera poses. Extensive experiments and ablation studies demonstrate the validity of D2T and its design choices, achieving state-of-the-art performance in both tasks of novel view synthesis and pose estimation while keeping high efficiency. Codes will be publicly available.

*Corresponding authors.

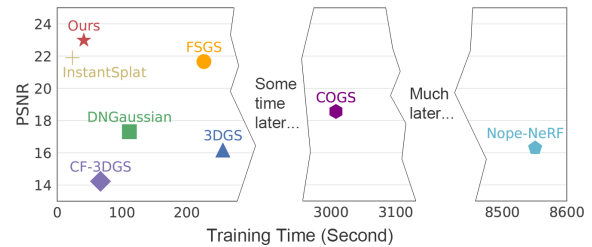


Figure 1. **Relationship Between Training Time and PSNR.** We show the training time and PSNR on Tanks and Temples dataset with three input views. Our method is Pareto-optimal on the efficiency-accuracy trade-off when compared to existing baselines.

1. Introduction

Photo-realistic scene reconstruction is a fundamental task in computer vision and graphics, with applications spanning Augmented Reality (AR) [86], Virtual Reality (VR) [31], autonomous navigation systems [34], and beyond [9]. Accurate 3D reconstruction enables immersive and interactive experiences, as well as precise spatial understanding in various real-world scenarios. In recent years, significant advancements have been achieved [4, 45, 57, 85], pushing the boundaries of what can be achieved in terms of rendering quality and geometric accuracy.

However, despite this progress, existing methods face significant challenges when dealing with real-world conditions. In particular, current approaches can be broadly categorized into two main types: **Sparse-View** methods and **SfM-free** methods. Sparse-view methods [19, 28, 36, 37, 74, 77, 82, 91] rely on accurately known camera poses and aim to reconstruct scenes from a limited number of images, but they often struggle when pose estimation is inaccurate or unavailable. On the other hand, SfM-free methods [7, 22, 72] jointly estimate camera poses and reconstruct scenes without requiring prior pose information, but most of them depend heavily on densely captured images

and perform poorly when only sparse inputs are available. Some works try to reduce the number of views by using long-range information [30, 59] or initializing from Multi-View Stereo model [20], but they suffer from long training time or poor rendering quality at novel viewpoints. Both approaches, while effective in specific situations, have limitations in real-world more practical settings where the input images are both sparse and uncalibrated.

To overcome this limitation, we propose a novel **coarse-to-fine framework** that combines the advantages of both Sparse-View and SfM-free methods, while addressing their respective weaknesses. Our method, named **Dust to Tower (D2T)**, enables efficient and photo-realistic scene reconstruction from sparse, uncalibrated images (without requiring intrinsic or extrinsic camera parameters) by first constructing a coarse model and then refining it through meticulously warped, and flaw-inpainted images at novel viewpoints. D2T leverages the efficiency of sparse methods while simultaneously solving for camera poses, as done in SfM-free methods, but without the need for densely captured images.

Our framework consists of three key modules: (1) A **Coarse Construction Module (CCM)** that initializes a 3D Gaussian Splatting (3DGS) model and recovers coarse camera poses using a fast Multi-View Stereo (MVS) model, narrowing the solution space for pose optimization. (2) A **Confidence Aware Depth Alignment (CADA)** module that refines depth maps by aligning inverse depths from a mono-depth model with coarse depths, ensuring accurate warping of images to novel viewpoints. (3) A **Warped Image-Guided Inpainting (WIGI)** module that warps input images to novel viewpoints and uses a lightweight inpainting model to fill in the missing regions (called holes), providing high-quality supervision for further refinement of the 3D model and the camera poses.

Extensive experiments demonstrate that **D2T** achieves state-of-the-art results in both rendering quality and pose estimation accuracy while maintaining high efficiency, as shown in Fig. 1. Our contributions can be summarized as follows:

- We introduce **D2T**, a novel coarse-to-fine framework that jointly optimizes 3DGS and camera poses from sparse, uncalibrated images, achieving superior rendering fidelity and efficiency.
- We propose **CADA**, a novel depth alignment technique that enhances warping accuracy by aligning mono-depth predictions with coarse depth estimates.
- We develop the **WIGI** module, which generates multi-view consistent images at novel viewpoints using efficient image warping and inpainting techniques.
- Extensive experimental evaluations on multiple datasets demonstrate the state-of-the-art performance of **D2T** in both novel view synthesis and camera pose estimation,

while keeping high efficiency.

2. Related Work

2.1. Photo-Realistic Scene Reconstruction

Photo-Realistic Scene Reconstruction is a long-standing problem in computer vision and graphics community [13, 55] and various representations have been explored to address this challenge, including meshes [24, 27, 51], light field [32, 70], planes [25, 65] and point clouds [2, 90].

Recent advancements in neural rendering techniques have highlighted Neural Radiance Field (NeRF) [45, 61] for remarkable ability to produce Photo-Realistic renderings. NeRF uses Multilayer Perceptron (MLP) to represent a 3D scene and images are rendered via volume rendering. However, NeRFs are limited by both training and rendering speed and suffer from artifacts. Substantial follow-ups aim at enhancing either the rendering quality [4–6, 56, 64, 68, 87] or the time efficiency [21, 23, 42, 46, 50, 56], but achieving both goals simultaneously is still challenging. More recently, 3D Gaussian Splatting (3DGS) [57] has shown a significant breakthrough in efficiency and rendering quality for complex real-world scenes. 3DGS represents a scene by a set of anisotropic 3D Gaussian primitives explicitly and enables real-time rendering with a differentiable splatting.

Despite the success of 3DGS in multiple 3D downstream tasks [1, 14, 33, 39, 62] and the improvement of rendering quality [16, 78, 85], the reliance on dense training images and scene information (*i.e.* precise camera parameters and scene point clouds) severely restricts its practical application. Motivated by the above issues, we design an efficient and effective framework for photo-realistic scene reconstruction from sparse and uncalibrated images.

2.2. Sparse-View Scene Reconstruction

Various studies attempt to reconstruct a Photo-Realistic scene using only sparse-view images. Some works [18, 19, 37, 66] use depth priors as additional geometric constraints on input views to mitigate overfitting. But they still underperform due to the lack of supervision from novel viewpoints. DietNeRF [28] proposes to supervise at unseen viewpoints by enforcing semantic consistency between training images and rendered images at unseen viewpoints using CLIP [49]. SinNeRF [77] further improves it by using the CLS token from DINO-VIT [10]. SparseGS [76] utilize SDS loss [48] to distill prior knowledge from pre-trained 2D diffusion model [53]. However, these methods often fail to capture local fine structures. Some methods [36, 82, 91] transform input views to unobserved viewpoints to supervise the renderings. Yet, the transformed images have many invisible regions (holes) due to view direction change and local image expansion. So only limited additional information is introduced, resulting in mi-

nor improvement. Recent studies use the powerful generative models to produce images at novel viewpoints as pseudo ground truths [41, 74, 83, 84] or enhance the renderings [43]. But they need complex condition networks to control the generative models, resulting in high computational costs. Other works [12, 15, 26, 29, 38, 73, 80, 88] train networks to directly output 3D model parameters are also related.

In summary, although achieving some improvement, prior sparse-view works are either hard to provide effective regularization to mitigate the overfitting or suffering from time efficiency. Therefore, we propose the CADA and the WIGI to efficiently generate high-quality supervision at novel viewpoints, resulting in better reconstruction quality.

2.3. SfM-free Scene Reconstruction

Sparse view methods typically rely on precise camera parameters obtained through time-consuming SfM processes (e.g., Colmap [54]), which often fail with limited images. To eliminate the dependence on SfM, NeRFmm [72] optimize the NeRF and camera parameters jointly, but it is limited to forward-facing scenes. Following NeRFmm, various initiatives have been pursued, including coarse-to-fine positional encoding strategy for camera poses [40], progressive optimization strategy [22, 44], Gaussian-MLPs for effective pose optimization [17], and depth-based regularization [7]. While some promising results have been achieved, they generally require dense captured images or/and rough initial poses, and take hours for optimizing a scene. COGS [30] and CG-3DGS [59] incorporate long-range information using image matching networks [8, 58] to reduce training views, but they still suffer from training efficiency. More recently, InstantSplat [20] uses a pre-trained MVS model [69] to initialize the 3DGS and image poses, and drops the Adaptive Density Control for time efficiency. However, the lack of supervision at novel viewpoints still impedes the reconstruction quality, resulting in blurred artifacts.

Our work is fundamentally different from existing works in these ways: 1) we propose a coarse-to-fine framework that first constructs a coarse 3D model from sparse and uncalibrated images, then further refine it by warped and inpainted images at novel viewpoints. 2) Comprehensive experiments on both object-level and scene-level datasets show leading performance and efficiency.

3. Method

3.1. Overview

Given sparse and uncalibrated images $\mathbf{I} = \{\mathbf{I}_i\}$ for $i \in \{1, 2, \dots, N\}$, our task is to reconstruct a photo-realistic 3D model \mathcal{G} for rendering novel views at unseen viewpoints and recover the camera parameters (*i.e.* intrinsic \mathbf{K} and poses $\mathbf{T} = \{\mathbf{T}_i\}$ for $i \in \{1, 2, \dots, N\}$). We assume a shared \mathbf{K}

for all views and use 3DGS as the 3D model representation. Our core contribution is to construct a coarse model efficiently and refine it using images at novel viewpoints generated by a warping-and-inpainting paradigm. The overview of the proposed method is illustrated in Fig. 2. We first introduce the Coarse Construction Module in Sec. 3.2. Next, we introduce the Confidence Aware Depth Alignment in Sec. 3.3, which refines the coarse depth maps for accurate warping. Sec. 3.4 presents the Warped Image-Guided Inpainting module that generates high-quality images at novel viewpoints used to refine the 3D model. Finally, we detail the joint optimization of Poses and 3DGS in Sec. 3.5.

3.2. Coarse Construction Module (CCM)

Instead of the SfM pre-processing, we propose to employ an efficient dense stereo model, *i.e.* DUS3R [69] to first predict pair-wise pointmaps, then align them into a global point cloud χ and solve the coarse camera parameters (*i.e.* \mathbf{K} and \mathbf{T}). Then, we optimize the poses and 3DGS simultaneously for a few steps to construct a coarse 3DGS. Specifically, DUS3R takes two images $\mathbf{I}_1, \mathbf{I}_2 \in \mathbb{R}^{H \times W \times 3}$ with the longer side not exceeding 512 pixels as input, and output two corresponding pointmaps $X_{1,1}, X_{2,1} \in \mathbb{R}^{H \times W \times 3}$ in the coordinate frame of \mathbf{I}_1 and confidence maps $C_{1,1}, C_{2,1} \in \mathbb{R}^{H \times W}$ in milliseconds.

We assume a simple pinhole camera model with a centered principal point, then we solve the only unknown parameter in camera intrinsic, *i.e.* the focal length f^* using Weiszfeld algorithm [47]:

$$f^* = \arg \min_f \sum_{i=0}^W \sum_{j=0}^H C_{1,1}^{i,j} \left\| (i', j') - f \frac{(X_{1,1}^{i,j,0}, X_{1,1}^{i,j,1})}{X_{1,1}^{i,j,2}} \right\| \quad (1)$$

with $i' = i - \frac{W}{2}$ and $j' = j - \frac{H}{2}$. As all images share the same camera model, we average the estimated focal lengths of all images to construct the camera intrinsic \mathbf{K} .

As DUS3R can only deal with image pairs and the scales of the pointmaps are inconsistent between different image pairs, we align multiple pointmaps into a common coordinate frame. Similar to [69], we first construct a complete connectivity graph $\mathcal{K}_N(\mathcal{V}, \mathcal{E})$ of all the N input images, where vertices \mathcal{V} are images and each edge $e = (n, m) \in \mathcal{E}$ indicates an image pair of \mathbf{I}_n and \mathbf{I}_m . We input every image pair $e = (n, m)$ to DUS3R, resulting the pair-wise predictions $X_{n,n}, X_{m,n}$ and $C_{n,n}, C_{m,n}$. To ensure clarity, we define $X_{n,e} := X_{n,n}$ and $X_{m,e} := X_{m,n}$. To align all pointmaps, we introduce a transformation matrix \mathbf{T}_e and scaling factor σ_e for each pair $e \in \mathcal{E}$ and optimize the global point cloud χ as following:

$$\chi^* = \arg \min_{\chi, \mathbf{T}, \sigma} \sum_{e \in \mathcal{E}} \sum_{v \in \mathcal{V}[e]} \sum_{i=1}^{HW} C_{v,e}^i \|\chi_v^i - \sigma_e \mathbf{T}_e X_{v,e}^i\| \quad (2)$$

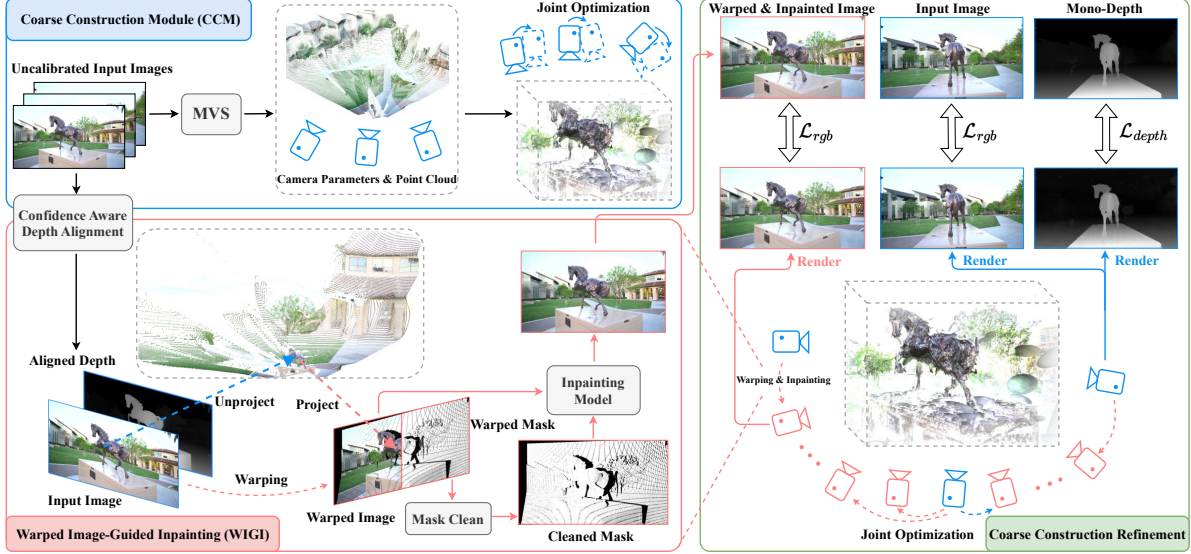


Figure 2. **Overview of D2T.** Given sparse-view and uncalibrated images, the Coarse Construction Module (CCM) first employs an efficient MVS method [69] to construct a coarse point cloud and rough camera poses to initialize a 3DGS. The initial 3DGS and poses are optimized simultaneously using the input images for a few steps (Sec. 3.2). To refine the model at novel viewpoints, a Confidence Aware Depth Alignment (CADA) module is proposed to enhance the warping accuracy by aligning relative inverse depth from a SOTA mono-depth model (Sec. 3.3). Then, we propose a Warped Image-Guided Inpainting (WIGI) module to warp input images to unseen viewpoints and inpaint the missing part in the warped images by a lightweight inpainting model (Sec. 3.4). Finally, 3DGS and poses are further refined by the inpainted images at novel viewpoints.

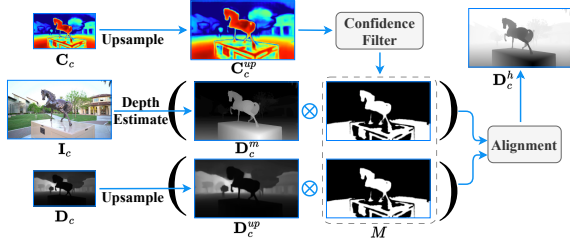


Figure 3. **Overview of the Confidence Aware Depth Alignment.** We align the mono-depth D_c^m to the reliable part of the coarse depth D_c^{up} , resulting in high quality depth map D_c^h .

Here, $\mathcal{V}[e] = \{n, m\}$ if $e = (n, m)$. The idea is that, for each pair e , the same rigid transformation \mathbf{T}_e should align both pointmaps $X_{n,e}$ and $X_{m,e}$ with the world-coordinate pointmaps χ_n and χ_m . To avoid the trivial solution $\sigma_e = 0$, for all $e \in \mathcal{E}$, we enforce $\Pi_e \sigma_e = 1$. We directly optimize the global camera poses $\mathbf{T} = \{\mathbf{T}_n\}$ by reparameterization:

$$\chi_n^{i,j} := \mathbf{T}_n^{-1} h(\mathbf{K}^{-1}[iD_n^{i,j}, jD_n^{i,j}, D_n^{i,j}]^T) \quad (3)$$

D_n is the depth map and $h(\cdot)$ denotes the homogeneous coordinates. i and j are the pixel coordinates. The optimization is carried out using standard gradient descent and typically converges within mere seconds on a standard GPU. We use the aligned point cloud χ to initialize the 3DGS and optimize the poses and 3DGS jointly for a few steps to set up a valid skeleton, which will be detailed in Sec. 3.5.

3.3. Confidence Aware Depth Alignment (CADA)

Warping train images to novel viewpoints relies on precise depth information. Previous methods [36, 76, 82] exploit the rendered depth maps for warping, but the rendered depth maps are inaccurate, since it is the expected depth maps and the 3D model is still rough during training. Directly upsampling the coarse and low-resolution depth maps from CCM may also introduce many noises. To address this issue, we propose using DepthAnything V2 (DAV2) [79] to estimate precise monocular relative inverse depth maps (abbreviated as mono-depth) and align it with the coarse depth maps.

The overview of CADA is illustrated in Fig. 3. Given a training image $\mathbf{I}_c \in \mathbb{R}^{H_h \times W_h \times 3}$ and corresponding coarse depth map $\mathbf{D}_c \in \mathbb{R}^{H_h \times W_h}$, we predict the mono-depth $\mathbf{D}_c^m \in \mathbb{R}^{H_h \times W_h}$ by DAV2 and upsample \mathbf{D}_c to $\mathbf{D}_c^{up} \in \mathbb{R}^{H_h \times W_h}$ via bilinear interpolation. The scale a and shift b between \mathbf{D}_c^m and \mathbf{D}_c^{up} are solved by a least squares problem. To improve alignment robustness, we use a mask M to retain only the reliable points for alignment, as uncertain depths in \mathbf{D}_c^m (e.g. in the sky) may cause misalignment. Specially, we generate a confidence map $C_c \in \mathbb{R}^{H_h \times W_h}$ for \mathbf{I}_c by taking the maximum value at position (i, j) across all confidence maps of \mathbf{I}_c from DUST3R. Upsample C_c gives $C_c^{up} \in \mathbb{R}^{H_h \times W_h}$, and retaining the top P percent value in C_c^{up} results in the Mask M . Finally, we estimate a and b :

$$(a, b) = \arg \min_{a,b} \sum_{i=1}^{H_h} \sum_{j=1}^{W_h} M(i, j) \left(\frac{1}{\mathbf{D}_c^{up}(i, j)} - (b + a\mathbf{D}_c^m(i, j)) \right)^2 \quad (4)$$

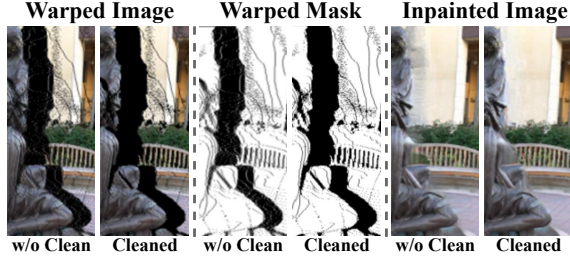


Figure 4. **Visualization of the Mask Clean.** Without Mask Clean, outliers in the warped image and warped mask can mislead the inpainting model, resulting in irrational results. The quality of inpainted images are improved after applying Mask Clean.

\mathbf{D}_c^m are aligned to \mathbf{D}_c^{up} , resulting in the aligned depth map: $\mathbf{D}_c^h = \frac{1}{b+a*\mathbf{D}_c^m}$.

3.4. Warped Image-Guided Inpainting (WIGI)

To alleviate the overfitting on input views and refine the model at unseen viewpoints, we propose a novel and efficient method to transform input images to novel viewpoints and fill the missing regions (holes) in warped images by inpainting. Specifically, given N sparse-view images, we sample $K^p * (N - 1)$ unseen poses \mathbf{T}^p using the B-Spline algorithm for comprehensive coverage of the scenarios. For an unseen pose \mathbf{T}_k^p , we warp the closest training image \mathbf{I}_c to \mathbf{T}_k^p using the aligned depth map \mathbf{D}_c^h of \mathbf{I}_c , resulting in the warped image \mathbf{I}_k^p and warped mask M_k^p . \mathbf{I}_k^p and M_k^p are used to guide the inpainting model [60] to eliminate the holes caused by the view direction change, as seen in Fig. 5.

Image warping with depths With the aligned depth map \mathbf{D}_c^h , we warp the input view \mathbf{I}_c at pose \mathbf{T}_c to the unseen viewpoint \mathbf{T}_k^p . The transform from \mathbf{T}_c to \mathbf{T}_k^p is given by: $\mathbf{T}_{kc} = (\mathbf{T}_k^p)^{-1}\mathbf{T}_c$. To warp \mathbf{I}_c to the unseen viewpoint \mathbf{T}_k^p , we first unproject \mathbf{I}_c with the aligned depth map \mathbf{D}_c^h to 3D space, then reproject it using the transform \mathbf{T}_{kc} and the intrinsic \mathbf{K} . Mathematically, the pixel location p_i in \mathbf{I}_c transforms to pixel location p_j in the novel view as:

$$p_j = \mathbf{K}\mathbf{T}_{kc}\mathbf{K}^{-1}\mathbf{D}_c^h(p_i)p_i \quad (5)$$

Then we can map the pixel colors from \mathbf{I}_c to the warped image \mathbf{I}_k^p by a flow field between p_i and p_j and generate a warp mask M_k^p to indicate the invalid pixels in \mathbf{I}_k^p . We use the Z-buffering [11] algorithm to resolve the projection ambiguities by retaining the point with the smallest depth when multiple points project to the same pixel location.

Holes Elimination by Inpainting After image warping, we have a warped image \mathbf{I}_k^p at unseen viewpoints, which often have holes due to view direction change and local expansion, as shown in Fig. 5. Previous methods [36, 76, 77, 91] mask out the missing region in warped image and only utilize the visible pixels to supervise the model. However, the

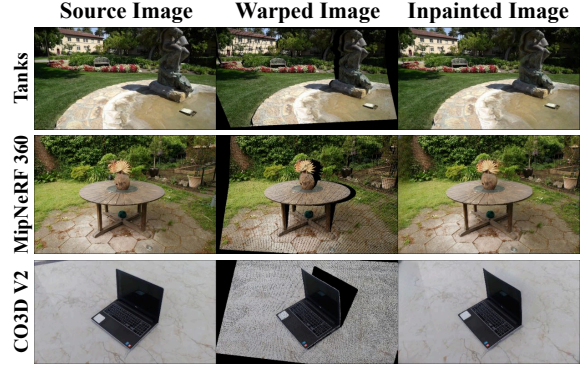


Figure 5. Visualization of the inpainting results. Tanks means the Tanks and Temples dataset.

visible pixels only provided limited additional constraints since they have participated in the optimization of the training views and the missing area is never known and remain unconstrained. To solve this issue, we propose to use the valid parts of the warped image to guide a lightweight inpainting model [60] \mathcal{P} to generate pixels in the missing regions. The inpainting model \mathcal{P} will fill the holes base on the visible content to make the output image natural and coherent. Given the warped image \mathbf{I}_k^p and warped mask M_k^p which indicates areas that need inpainting, a straightforward way is to directly apply the \mathbf{I}_k^p and M_k^p for inpainting: $\hat{\mathbf{I}}_k^p = \mathcal{P}(\mathbf{I}_k^p, M_k^p)$.

Mask Clean However, imperfect and distorted warpings near the edges (*i.e.* discontinuities in depth) can arise from erroneous geometry predicted by DAV2. Such outliers may mislead the model to misunderstand the scene and generate unreasonable content, as shown in Fig. 4. To solve this issue, we propose a simple yet effective method to clean the warped mask M_k^p : $\hat{M}_k^p = \mathcal{F}(M_k^p)$. Specifically, a point is deemed an outlier if it has less than $\frac{w \times w}{2}$ neighboring points within its $w \times w$ neighborhood. The final inpainted images are obtained as $\hat{\mathbf{I}}_k^p = \mathcal{P}(\mathbf{I}_k^p, \hat{M}_k^p)$, where \hat{M}_k^p indicates the valid and visible points. We can then use $\hat{\mathbf{I}}_k^p$ at the novel viewpoints \mathbf{T}_k^p to refine the 3DGS model.

Comparing to concurrent works [41, 74, 83, 84] which directly generate complete images at novel viewpoints using the pre-trained generative models [53, 67, 75], WIGI offers more robust multi-view consistency through explicit geometric correspondences and greater efficiency.

3.5. Joint Optimization of Poses and 3DGS

In this section, we first discuss the optimization of camera poses, then we present the loss function used for training. Finally, we detail the coarse-to-fine optimization strategy.

Pose Optimization We optimize the camera poses by adding tiny perturbations $\Delta\mathbf{T}$ to the initial poses \mathbf{T} . The

Category	Method	3 views				6 views				12 views			
		PSNR \uparrow	SSIM \uparrow	LPIPS \downarrow	Time \downarrow	PSNR \uparrow	SSIM \uparrow	LPIPS \downarrow	Time \downarrow	PSNR \uparrow	SSIM \uparrow	LPIPS \downarrow	Time \downarrow
Sparse	FSGS	21.66	0.719	0.263	3m 47s	<u>25.70</u>	0.825	0.208	3m 41s	<u>27.78</u>	<u>0.861</u>	0.196	3m 35s
	DNGaussian	17.31	0.534	0.400	1m 52s	22.05	0.719	0.292	2m 2s	24.38	0.785	0.270	2m 7s
	3DGS	16.17	0.558	0.366	4m 16s	19.30	0.725	0.241	5m 38s	22.48	0.808	0.179	7m 5s
Unpose	CF-3DGS	14.23	0.402	0.454	1m 7s	15.60	0.447	0.430	2m 10s	15.21	0.453	0.456	3m 34s
	Nope-NeRF	16.30	0.469	0.589	2h 22m	19.71	0.560	0.535	3h 14m	21.85	0.614	0.497	5h 17m
Unconstraint	InstantSplat	<u>21.90</u>	<u>0.749</u>	<u>0.218</u>	23s	25.07	<u>0.827</u>	<u>0.150</u>	28s	27.33	0.860	<u>0.129</u>	42s
	COGS	18.56	0.569	0.299	50m 8s	22.32	0.703	0.195	1h 19m	25.60	0.810	0.128	2h 13m
	Ours	23.39	0.776	0.164	<u>41s</u>	26.49	0.859	0.124	<u>49s</u>	27.93	0.888	0.113	<u>1m7s</u>

Table 1. NVS results on Tanks and Temples dataset. The best results are highlighted in bold and the second best results are underlined.

Category	Method	3 views				6 views				12 views			
		PSNR \uparrow	SSIM \uparrow	LPIPS \downarrow	Time \downarrow	PSNR \uparrow	SSIM \uparrow	LPIPS \downarrow	Time \downarrow	PSNR \uparrow	SSIM \uparrow	LPIPS \downarrow	Time \downarrow
Sparse	FSGS	12.33	0.261	0.637	3m 17s	14.18	0.339	0.584	3m 18s	<u>17.27</u>	0.477	0.507	3m 28s
	DNGaussian	11.37	0.235	0.694	2m 45s	13.19	0.348	0.639	2m 52s	14.43	0.402	0.622	2m 57s
	3DGS	11.56	0.188	0.625	6m 41s	13.06	0.261	0.575	7m 6s	14.88	<u>0.493</u>	<u>0.375</u>	7m 38s
Unpose	CF-3DGS	12.70	0.227	0.594	1m 10s	13.37	0.230	0.590	2m 19s	13.96	0.260	0.602	4m 2s
	Nope-NeRF	<u>14.43</u>	<u>0.304</u>	<u>0.702</u>	2h 12m	<u>15.86</u>	<u>0.351</u>	<u>0.685</u>	3h 7m	17.02	0.384	0.662	5h 1m
Unconstraint	InstantSplat	13.77	0.285	<u>0.551</u>	23s	15.34	<u>0.399</u>	<u>0.455</u>	30s	17.09	0.456	0.493	49s
	COGS	12.48	0.204	0.593	1h 7m	13.60	0.257	0.557	1h 44m	15.72	0.342	0.480	2h 28m
	Ours	14.99	0.331	0.524	<u>45s</u>	17.80	0.443	0.396	<u>53s</u>	19.73	0.501	0.354	<u>1m19s</u>

Table 2. NVS results on MipNeRF360 dataset. The best results are highlighted in bold and the second best results are underlined.

images and depths rendered at perturbed poses are expressed by: $\tilde{\mathbf{I}}, \tilde{\mathbf{D}} = \mathcal{R}(\mathcal{G}, \Delta \mathbf{T} \times \mathbf{T})$, where $\mathcal{R}(\cdot)$ refers to the rendering process. We update $\Delta \mathbf{T}$ using stochastic gradient descent alongside scene optimization to refine the poses of training images.

Loss Function Following 3DGS [57], we train the 3DGS by minimizing the difference between training images \mathbf{I} and rendering images $\tilde{\mathbf{I}}$ using stochastic gradient descent:

$$\mathcal{L}_{\text{rgb}} = (1 - \lambda)\mathcal{L}_1(\tilde{\mathbf{I}}, \mathbf{I}) + \lambda\mathcal{L}_{D\text{-SSIM}}(\tilde{\mathbf{I}}, \mathbf{I}) \quad (6)$$

To achieve coherent geometry, we introduce a geometry prior to the optimization. We use the predicted high-quality mono-depths \mathbf{D}^m as a depth prior. To avoid scale discrepancies, we convert the rendered depth maps $\tilde{\mathbf{D}}$ into inverse depth maps and use a loose constraint, Pearson correlation which measures the consistency between two variables for supervision. The loss $\mathcal{L}_{\text{depth}}$ is defined as follows:

$$\mathcal{L}_{\text{depth}} = 1 - \rho\left(\frac{1}{\tilde{\mathbf{D}}}, \mathbf{D}^m\right), \rho(X, Y) = \frac{\text{cov}(X, Y)}{\sigma_X \sigma_Y} \quad (7)$$

$\text{cov}(\cdot)$ denotes covariance. σ_X, σ_Y are standard deviation.

Coarse-to-Fine Optimization Strategy As noted in Sec. 3.4, the warping process requires accurate camera poses. Directly using the coarse poses from DUST3R may lead to declined performance. Thus, we propose a Coarse-to-Fine Optimization Strategy for more robust training.

In the coarse stage, we first train the coarse 3DGS model and poses from DUST3R using only the training views for k_1 steps. The loss function in the coarse stage is:

$$\mathcal{L}_c = \mathcal{L}_{\text{rgb}}(\mathbf{I}, \tilde{\mathbf{I}}) + \lambda_d \mathcal{L}_{\text{depth}}(\tilde{\mathbf{D}}, \mathbf{D}^m). \quad (8)$$

In the fine stage, we use the updated input image poses to perform WIGI (*i.e.* Sec. 3.4), resulting in $K^p \times (N - 1)$ images at novel viewpoints. We supervise the corresponding rendered images by \mathcal{L}_{rgb} as an additional regularization. We refine the 3DGS K_2 steps with the fine stage loss:

$$\mathcal{L}_f = \mathcal{L}_c + \lambda_{\text{pseudo}} \mathcal{L}_{\text{rgb}}(\hat{\mathbf{I}}^p, \tilde{\mathbf{I}}^p) \quad (9)$$

where $\tilde{\mathbf{I}}^p$ means the rendered images and $\hat{\mathbf{I}}^p$ is the warped and inpainted images at unseen viewpoints.

4. Experiments

4.1. Experiment Setup

Datasets We conduct extensive experiments on three datasets, encompassing both object and scene reconstruction scenarios. (1) **Tanks and Temples** [35] dataset is widely used. We use the same eight scenes for evaluation as used in [7, 30]. For each scene, we uniformly sample 24 images and then uniformly select 12 images from it (including the first and last images) as the training set, N sparse training views are sampled from the training set. The remaining 12 images are used for test. (2) **MipNeRF360** dataset [5] features complex central objects or areas against a detailed background. We use the published seven scenes for evaluation. We uniformly sample 24 images from the first 48 frames and split the train/test set similarly. (3) **CO3D V2** dataset [52] consists of thousands of videos with 360-degree coverage around central objects. We randomly select 8 videos of different objects and follow the same protocol to split the train/test set as the Tanks and Temples dataset.

Metrics We evaluate the tasks of **Novel View Syntheses** (NVS) and **Camera Pose Estimation**. For NVS, we report Peak Signal-to-Noise Ratio (PSNR), Structural Simi-

Category	Method	3 views				6 views				12 views			
		PSNR \uparrow	SSIM \uparrow	LPIPS \downarrow	Time \downarrow	PSNR \uparrow	SSIM \uparrow	LPIPS \downarrow	Time \downarrow	PSNR \uparrow	SSIM \uparrow	LPIPS \downarrow	Time \downarrow
Sparse	FSGS	17.99	0.731	0.438	4m 47s	20.35	0.770	0.395	5m 8s	22.32	0.802	0.367	5m 30s
	DNGaussian	15.17	0.703	0.476	5m 3s	17.04	0.738	0.441	5m 26s	20.31	0.796	0.389	5m 30s
	3DGS	16.10	0.662	0.458	8m 29s	18.59	0.722	0.419	9m 52s	19.96	0.762	0.387	11m 11s
Unpose	CF-3DGS	16.27	0.713	0.445	3m 30s	16.87	0.717	0.449	5m 53s	17.06	0.731	0.457	8m 39s
	InstantSplat	<u>18.15</u>	<u>0.741</u>	<u>0.362</u>	30s	<u>22.24</u>	<u>0.826</u>	<u>0.283</u>	37s	<u>25.75</u>	<u>0.869</u>	<u>0.242</u>	55s
Unconstraint	COGS	16.10	0.669	0.455	14m 39s	17.17	0.696	0.435	26m 4s	18.07	0.726	0.410	42m 3s
	Ours	19.79	0.771	0.345	<u>59s</u>	24.74	0.854	0.250	<u>1m 12s</u>	27.08	0.876	0.225	<u>1m 36s</u>

Table 3. NVS results on CO3D V2 dataset. The best results are highlighted in bold and the second best results are underlined.

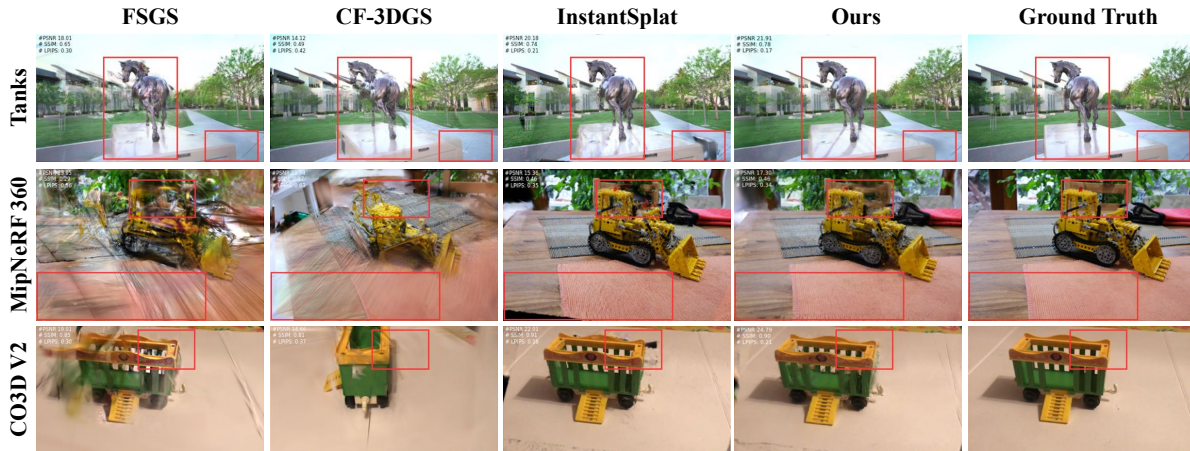


Figure 6. **Qualitative Results of Novel View Synthesis with three training views.** Our method produces more realistic rendering results with fewer artifacts than others, especially in the occluded regions. The evaluation metrics against ground truth are plot at the top and left of the images. Please zoom in for detail.

larity Index Measure (SSIM) [71], and Learned Perceptual Image Patch Similarity (LPIPS) [89]. For camera pose estimation, we align the estimated poses with the ground truth using the Umeyama algorithm [63] and report the Absolute Trajectory Error (ATE) and Relative Pose Error (RPE) following [7, 22]. For Tanks and Temples and MipNeRF360 datasets, we consider Colmap [54] poses as the ground truth. CO3D V2 provides its own ground truth poses.

Baselines We compare our method with three types of methods: 1) **Sparse methods** [37, 91], which reconstruct from sparse views but requires pre-computing camera parameters. We use ground truth parameters to train them. Vanilla 3DGS [57] is also evaluated as a baseline. 2) **Unpose methods** [7, 22] that reconstruct from uncalibrated images but requires dense captured images; 3) **Unconstraint methods** [20, 30] that reconstruct from sparse and uncalibrated images. We use their official codes and default configurations to train all methods and report the performance.

Implementation Details We develop our entire framework based on PyTorch [3] and use gsplat [81] for differentiable rendering. We follow the default optimization parameters of 3DGS [57] unless otherwise specified. All experiments are conducted on an Nvidia 4090 GPU. We construct the coarse solution with 300 iterations and refine the 3D model for another 1700 iterations. We set $K^p = 18, 6, 4$

for 3, 6, 12 training view settings, respectively. And we set $\lambda = 0.1, \lambda_d = 0.5, \lambda_{pseudo} = 0.3$ for all experiments. More details are provided in the supplementary material.

Test View Pose Alignment To evaluate the Novel View Synthesis performance, we need to render images at the same viewpoints as the test images. But the poses of the test images are unknown, we need to localize the test images in the trained 3DGS model. Inspired by NeRFmm [72], we first freeze the trained 3DGS model, and then optimize the camera poses of the test views via stochastic gradient descent. The optimization target is to minimize the photometric loss between the rendered images and the test views. We optimize 200 steps for each test view.

4.2. Evaluation on Novel View Synthesis

Tab. 1, Tab. 2, Tab. 3 report the averaged results and training time on Tanks and Temples, MipNeRF360 and CO3D V2 datasets, respectively. Our method consistently outperforms all baselines across all the datasets in the PSNR, SSIM, and LPIPS scores and achieves top-tier training efficiency, which strongly proves the effectiveness and robustness of our method. The qualitative results are shown in Fig 6. InstantSplat fails to reconstruct the occluded regions at novel viewpoints, resulting in holes. CF-3DGS and FSGS suffer from blurred artifacts due to the overfitting issue. Our method successfully reconstructs the missing part at novel

views	Dataset	Ours			COGS			CF-3DGS			Nope-NeRF			InstantSplat		
		RPE _r	RPE _t	ATE	RPE _r	RPE _t	ATE	RPE _r	RPE _t	ATE	RPE _r	RPE _t	ATE	RPE _r	RPE _t	ATE
3 views	Tanks	0.416	0.807	0.003	<u>1.105</u>	<u>3.809</u>	<u>0.017</u>	21.369	73.933	0.237	19.785	50.972	0.155	1.800	12.221	0.025
	Mipnerf	2.642	3.269	0.009	73.903	86.434	<u>0.187</u>	82.720	110.053	0.348	81.647	128.994	0.323	<u>23.104</u>	96.475	0.267
	CO3D	13.370	11.731	0.026	121.102	<u>100.196</u>	0.369	121.475	105.898	<u>0.280</u>	-	-	-	<u>103.141</u>	118.120	0.323
6 views	Tanks	0.222	0.364	0.003	<u>0.258</u>	<u>0.588</u>	<u>0.004</u>	7.412	23.579	0.172	6.002	15.278	0.114	1.221	5.459	0.025
	Mipnerf	7.146	5.940	0.022	53.527	<u>38.996</u>	<u>0.205</u>	61.405	49.423	0.303	61.791	107.246	0.547	<u>20.655</u>	55.885	0.281
	CO3D	5.569	7.203	0.054	64.521	42.951	0.320	<u>50.596</u>	<u>36.459</u>	<u>0.248</u>	-	-	-	97.642	50.471	0.280
12 views	Tanks	<u>0.490</u>	0.194	0.002	0.119	<u>0.299</u>	<u>0.004</u>	2.553	7.075	0.099	2.162	7.147	0.111	0.886	2.128	0.015
	Mipnerf	1.896	1.613	0.012	23.839	<u>14.940</u>	<u>0.149</u>	29.861	19.974	0.216	29.865	58.931	0.541	<u>13.632</u>	26.620	0.207
	CO3D	2.787	2.810	0.039	36.361	18.785	0.203	<u>22.164</u>	<u>13.539</u>	<u>0.171</u>	-	-	-	22.644	45.430	0.207

Table 4. **Pose Estimation Evaluation results.** The RPE_t is scaled by 100, the RPE_r is in degree and the ATE is in the ground truth scale. The best results are highlighted in bold and the second best results are underlined.

viewpoints, and the rendered images are more clearer and with fewer artifacts.

4.3. Evaluation on Camera Pose Estimation

We report the pose estimation results of three datasets in Tab. 4. Our approach achieves new state-of-the-art performance for most evaluation metrics, demonstrating the effectiveness of our method. Notably, our method is more accurate than the compared methods by an order of magnitude in ATE, and the RPE_r and RPE_t are also significantly improved across all scenarios. CF-3DGS and Nope-NeRF rely on dense input and struggle to estimate accurate camera poses in sparse-view settings.

4.4. Ablation Study

To fully understand the design choices in our method, we conduct ablation studies on the Tanks and Temples dataset with three training views. The results are shown in Tab. 5.

Impact of CADA The variant (a) removes the CADA module and directly uses the upsampled coarse depth maps for warping. It makes the warping process inaccurate, resulting in declined reconstruction quality.

Effectiveness of WIGI As shown in Tab. 5 (b), omitting WIGI results in a significant performance drop, since the unseen regions lack supervision. Besides, the variant (c) ablates the inpainting step and directly uses the warped images for supervision, leading to noticeably declined results. It validates the necessity of the inpainting process, which distinguishes our method from prior warping-based methods. The Mask Clean also contributes to the rendering quality, as evidenced by the results of variant (d).

Joint Optimization of Poses and 3DGS Matters Variant (e) disables the optimization of camera poses, and uses the initial camera poses from DUST3R to perform WIGI and train the 3DGS. As shown in Tab. 5, it leads to declined pose accuracy, the rendering quality is also impeded due to the inaccurate camera poses. The Coarse-to-Fine Optimization Strategy is also critical to the reconstruction quality, proved by the results of variant (f).

Variant	PSNR \uparrow	SSIM \uparrow	RPE _t \downarrow	RPE _r \downarrow
(a) w/o CADA	22.89	0.7632	0.8253	0.4189
(b) w/o WIGI	22.18	0.7511	0.8101	0.4175
(c) w/o Inpainting	22.29	0.7550	0.8223	0.4162
(d) w/o Mask Clean	22.90	0.7666	0.8122	0.4193
(e) w/o Joint Optimization	22.69	0.7547	1.4681	0.4526
(f) w/o Coarse-to-Fine Strategy	22.85	0.7621	1.0384	0.4261
Full	23.39	0.7762	0.8068	0.4159

Table 5. Ablation study on Tanks and Temples dataset with three training views.

Impact of the number of inpainting views We present PSNR results for varying numbers of inpainting views on the Tanks and Temples dataset with three input views, as demonstrated in Fig. 7. Initially, the PSNR significantly improves due to the inclusion of warped and inpainted images. As K^p increases, the improvement in PSNR becomes marginal.

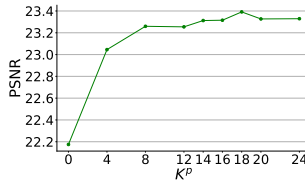


Figure 7. Impact of the number of inpainting views

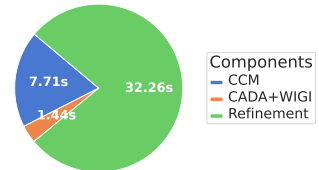


Figure 8. Time Analyses of Different Components.

Time Analyses Fig. 8 shows the average time consumption of different modules, which is tested on the Tanks and Temples dataset with three training views. We set $K^p = 18$, resulting in 36 warped and inpainted images in total. Our proposed CCM can construct a coarse 3D model and recover initial camera poses in mere seconds. It only takes 1.44s to generate 36 warped and inpainted images, proving the efficiency of the proposed CADA and WIGI.

5. Conclusion

In this paper, we propose D2T, a novel coarse-to-fine framework that aims to use sparse and uncalibrated images for photo-realistic scene reconstruction. Starting from sparse and uncalibrated images, D2T first constructs a coarse solution efficiently by CCM. To refine the 3D

model at novel viewpoints, we propose CADA and WIGI to generate images at novel viewpoints by warping and inpainting, which is proven effective and efficient in enhancing the rendering quality at novel viewpoints. Extensive experimental results on three datasets show that D2T achieves state-of-the-art results in both NVS and pose estimation with high efficiency. However, the alignment of a global point cloud limited D2T to reconstruct large-scale scenes with hundreds of input images. An incremental alignment paradigm will be explored in future research.

References

- [1] Rameen Abdal, Yifan Wang, Zifan Shi, Yinghao Xu, Ryan Po, Zhengfei Kuang, Qifeng Chen, Dit-Yan Yeung, and Gordon Wetzstein. Gaussian shell maps for efficient 3d human generation. In *IEEE/CVF Conference on Computer Vision and Pattern Recognition, CVPR 2024, Seattle, WA, USA, June 16-22, 2024*, pages 9441–9451. IEEE, 2024. 2
- [2] Kara-Ali Aliev, Artem Sevastopolsky, Maria Kolos, Dmitry Ulyanov, and Victor S. Lempitsky. Neural point-based graphics. In *Computer Vision - ECCV 2020 - 16th European Conference, Glasgow, UK, August 23-28, 2020, Proceedings, Part XXII*, pages 696–712. Springer, 2020. 2
- [3] Jason Ansel, Edward Yang, Horace He, Natalia Gimelshein, Animesh Jain, Michael Voznesensky, Bin Bao, Peter Bell, David Berard, Evgeni Burovski, Geeta Chauhan, Anjali Chourdia, Will Constable, Alban Desmaison, Zachary DeVito, Elias Ellison, Will Feng, Jiong Gong, Michael Gschwind, Brian Hirsh, Sherlock Huang, Kshiteej Kalambarakar, Laurent Kirsch, Michael Lazos, Mario Lezcano, Yanbo Liang, Jason Liang, Yinghai Lu, CK Luk, Bert Maher, Yunjie Pan, Christian Puhrsch, Matthias Reso, Mark Saroufim, Marcos Yukio Siraichi, Helen Suk, Michael Suo, Phil Tillet, Eikan Wang, Xiaodong Wang, William Wen, Shunting Zhang, Xu Zhao, Keren Zhou, Richard Zou, Ajit Mathews, Gregory Chanan, Peng Wu, and Soumith Chintala. PyTorch 2: Faster Machine Learning Through Dynamic Python Bytecode Transformation and Graph Compilation. In *29th ACM International Conference on Architectural Support for Programming Languages and Operating Systems, Volume 2 (ASPLOS '24)*. ACM, 2024. 7
- [4] Jonathan T. Barron, Ben Mildenhall, Dor Verbin, Pratul P. Srinivasan, and Peter Hedman. Mip-nerf 360: Unbounded anti-aliased neural radiance fields. In *IEEE/CVF Conference on Computer Vision and Pattern Recognition, CVPR 2022, New Orleans, LA, USA, June 18-24, 2022*, pages 5460–5469. IEEE, 2022. 1, 2
- [5] Jonathan T. Barron, Ben Mildenhall, Dor Verbin, Pratul P. Srinivasan, and Peter Hedman. Mip-nerf 360: Unbounded anti-aliased neural radiance fields. In *IEEE/CVF Conference on Computer Vision and Pattern Recognition, CVPR 2022, New Orleans, LA, USA, June 18-24, 2022*, pages 5460–5469. IEEE, 2022. 6
- [6] Jonathan T. Barron, Ben Mildenhall, Dor Verbin, Pratul P. Srinivasan, and Peter Hedman. Zip-nerf: Anti-aliased grid-based neural radiance fields. In *IEEE/CVF International Conference on Computer Vision, ICCV 2023, Paris, France, October 1-6, 2023*, pages 19640–19648. IEEE, 2023. 2
- [7] Wenjing Bian, Zirui Wang, Kejie Li, and Jia-Wang Bian. Nope-nerf: Optimising neural radiance field with no pose prior. In *IEEE/CVF Conference on Computer Vision and Pattern Recognition, CVPR 2023, Vancouver, BC, Canada, June 17-24, 2023*, pages 4160–4169. IEEE, 2023. 1, 3, 6, 7
- [8] Xudong Cai, Yongcai Wang, Lun Luo, Minhong Wang, Deying Li, Jintao Xu, Weihao Gu, and Rui Ai. PRISM: progressive dependency maximization for scale-invariant image matching. *CoRR*, abs/2408.03598, 2024. 3
- [9] Yuanhao Cai, Yixun Liang, Jiahao Wang, Angtian Wang, Yulun Zhang, Xiaokang Yang, Zongwei Zhou, and Alan L. Yuille. Radiative gaussian splatting for efficient x-ray novel view synthesis. In *Computer Vision - ECCV 2024 - 18th European Conference, Milan, Italy, September 29-October 4, 2024, Proceedings, Part I*, pages 283–299. Springer, 2024. 1
- [10] Mathilde Caron, Hugo Touvron, Ishan Misra, Hervé Jégou, Julien Mairal, Piotr Bojanowski, and Armand Joulin. Emerging properties in self-supervised vision transformers. In *2021 IEEE/CVF International Conference on Computer Vision, ICCV 2021, Montreal, QC, Canada, October 10-17, 2021*, pages 9630–9640. IEEE, 2021. 2
- [11] Edwin Catmull. *A Subdivision Algorithm for Computer Display of Curved Surfaces*. PhD thesis, University of Utah, Department of Computer Science, Salt Lake City, Utah, U.S.A., 1974. 5
- [12] David Charatan, Sizhe Lester Li, Andrea Tagliasacchi, and Vincent Sitzmann. Pixelsplat: 3d gaussian splats from image pairs for scalable generalizable 3d reconstruction. In *IEEE/CVF Conference on Computer Vision and Pattern Recognition, CVPR 2024, Seattle, WA, USA, June 16-22, 2024*, pages 19457–19467. IEEE, 2024. 3
- [13] Shenchang Eric Chen and Lance Williams. View interpolation for image synthesis. In *Proceedings of the 20th Annual Conference on Computer Graphics and Interactive Techniques, SIGGRAPH 1993, Anaheim, CA, USA, August 2-6, 1993*, pages 279–288. ACM, 1993. 2
- [14] Yiwen Chen, Zilong Chen, Chi Zhang, Feng Wang, Xiaofeng Yang, Yikai Wang, Zhongang Cai, Lei Yang, Huaping Liu, and Guosheng Lin. Gaussianeditor: Swift and controllable 3d editing with gaussian splatting. In *IEEE/CVF Conference on Computer Vision and Pattern Recognition, CVPR 2024, Seattle, WA, USA, June 16-22, 2024*, pages 21476–21485. IEEE, 2024. 2
- [15] Yuedong Chen, Haofei Xu, Chuanxia Zheng, Bohan Zhuang, Marc Pollefeys, Andreas Geiger, Tat-Jen Cham, and Jianfei Cai. Mvsplat: Efficient 3d gaussian splatting from sparse multi-view images. *CoRR*, abs/2403.14627, 2024. 3
- [16] Kai Cheng, Xiaoxiao Long, Kaizhi Yang, Yao Yao, Wei Yin, Yuexin Ma, Wenping Wang, and Xuejin Chen. Gaussianpro: 3d gaussian splatting with progressive propagation. In *Forty-first International Conference on Machine Learning, ICML 2024, Vienna, Austria, July 21-27, 2024*. OpenReview.net, 2024. 2
- [17] Shin-Fang Chng, Sameera Ramasinghe, Jamie Sherrah, and Simon Lucey. GARF: gaussian activated radiance fields

- for high fidelity reconstruction and pose estimation. *CoRR*, abs/2204.05735, 2022. 3
- [18] Jaeyoung Chung, Jeongtaek Oh, and Kyoung Mu Lee. Depth-regularized optimization for 3d gaussian splatting in few-shot images. In *IEEE/CVF Conference on Computer Vision and Pattern Recognition, CVPR 2024 - Workshops, Seattle, WA, USA, June 17-18, 2024*, pages 811–820. IEEE, 2024. 2
- [19] Kangle Deng, Andrew Liu, Jun-Yan Zhu, and Deva Ramanan. Depth-supervised nerf: Fewer views and faster training for free. In *IEEE/CVF Conference on Computer Vision and Pattern Recognition, CVPR 2022, New Orleans, LA, USA, June 18-24, 2022*, pages 12872–12881. IEEE, 2022. 1, 2
- [20] Zhiwen Fan, Wenyan Cong, Kairun Wen, Kevin Wang, Jian Zhang, Xinghao Ding, Danfei Xu, Boris Ivanovic, Marco Pavone, Georgios Pavlakos, Zhangyang Wang, and Yue Wang. Instantsplat: Unbounded sparse-view pose-free gaussian splatting in 40 seconds. *CoRR*, abs/2403.20309, 2024. 2, 3, 7
- [21] Sara Fridovich-Keil, Alex Yu, Matthew Tancik, Qinhong Chen, Benjamin Recht, and Angjoo Kanazawa. Plenoxels: Radiance fields without neural networks. In *IEEE/CVF Conference on Computer Vision and Pattern Recognition, CVPR 2022, New Orleans, LA, USA, June 18-24, 2022*, pages 5491–5500. IEEE, 2022. 2
- [22] Yang Fu, Xiaolong Wang, Sifei Liu, Amey Kulkarni, Jan Kautz, and Alexei A. Efros. Colmap-free 3d gaussian splatting. In *IEEE/CVF Conference on Computer Vision and Pattern Recognition, CVPR 2024, Seattle, WA, USA, June 16-22, 2024*, pages 20796–20805. IEEE, 2024. 1, 3, 7
- [23] Stephan J. Garbin, Marek Kowalski, Matthew Johnson, Jamie Shotton, and Julien P. C. Valentin. Fastnerf: High-fidelity neural rendering at 200fps. In *2021 IEEE/CVF International Conference on Computer Vision, ICCV 2021, Montreal, QC, Canada, October 10-17, 2021*, pages 14326–14335. IEEE, 2021. 2
- [24] Yuan-Chen Guo, Yan-Pei Cao, Chen Wang, Yu He, Ying Shan, and Song-Hai Zhang. Vmesh: Hybrid volume-mesh representation for efficient view synthesis. In *SIGGRAPH Asia 2023 Conference Papers, SA 2023, Sydney, NSW, Australia, December 12-15, 2023*, pages 17:1–17:11. ACM, 2023. 2
- [25] Derek Hoiem, Alexei A. Efros, and Martial Hebert. Automatic photo pop-up. *ACM Trans. Graph.*, 24(3):577–584, 2005. 2
- [26] Yicong Hong, Kai Zhang, Jiuxiang Gu, Sai Bi, Yang Zhou, Difan Liu, Feng Liu, Kalyan Sunkavalli, Trung Bui, and Hao Tan. LRM: large reconstruction model for single image to 3d. In *The Twelfth International Conference on Learning Representations, ICLR 2024, Vienna, Austria, May 7-11, 2024*. OpenReview.net, 2024. 3
- [27] Ronghang Hu, Nikhila Ravi, Alexander C. Berg, and Deepak Pathak. Worldsheet: Wrapping the world in a 3d sheet for view synthesis from a single image. In *2021 IEEE/CVF International Conference on Computer Vision, ICCV 2021, Montreal, QC, Canada, October 10-17, 2021*, pages 12508–12517. IEEE, 2021. 2
- [28] Ajay Jain, Matthew Tancik, and Pieter Abbeel. Putting nerf on a diet: Semantically consistent few-shot view synthesis. In *2021 IEEE/CVF International Conference on Computer Vision, ICCV 2021, Montreal, QC, Canada, October 10-17, 2021*, pages 5865–5874. IEEE, 2021. 1, 2
- [29] Hanwen Jiang, Qixing Huang, and Georgios Pavlakos. Real3d: Scaling up large reconstruction models with real-world images. *CoRR*, abs/2406.08479, 2024. 3
- [30] Kaiwen Jiang, Yang Fu, Mukund Varma T., Yash Belhe, Xiaolong Wang, Hao Su, and Ravi Ramamoorthi. A construct-optimize approach to sparse view synthesis without camera pose. In *ACM SIGGRAPH 2024 Conference Papers, SIGGRAPH 2024, Denver, CO, USA, 27 July 2024- 1 August 2024*, page 124. ACM, 2024. 2, 3, 6, 7
- [31] Ying Jiang, Chang Yu, Tianyi Xie, Xuan Li, Yutao Feng, Huamin Wang, Minchen Li, Henry Y. K. Lau, Feng Gao, Yin Yang, and Chenfanfu Jiang. VR-GS: A physical dynamics-aware interactive gaussian splatting system in virtual reality. In *ACM SIGGRAPH 2024 Conference Papers, SIGGRAPH 2024, Denver, CO, USA, 27 July 2024- 1 August 2024*, page 78. ACM, 2024. 1
- [32] Nima Khademi Kalantari, Ting-Chun Wang, and Ravi Ramamoorthi. Learning-based view synthesis for light field cameras. *ACM Trans. Graph.*, 35(6):193:1–193:10, 2016. 2
- [33] Nikhil Varma Keetha, Jay Karhade, Krishna Murthy Jatavallabhula, Gengshan Yang, Sebastian Scherer, Deva Ramanan, and Jonathon Luiten. Splatam: Splat, track & map 3d gaussians for dense RGB-D SLAM. In *IEEE/CVF Conference on Computer Vision and Pattern Recognition, CVPR 2024, Seattle, WA, USA, June 16-22, 2024*, pages 21357–21366. IEEE, 2024. 2
- [34] Mustafa Khan, Hamidreza Fazlali, Dhruv Sharma, Tongtong Cao, Dongfeng Bai, Yuan Ren, and Bingbing Liu. Autosplat: Constrained gaussian splatting for autonomous driving scene reconstruction. *CoRR*, abs/2407.02598, 2024. 1
- [35] Arno Knapitsch, Jaesik Park, Qian-Yi Zhou, and Vladlen Koltun. Tanks and temples: benchmarking large-scale scene reconstruction. *ACM Trans. Graph.*, 36(4):78:1–78:13, 2017. 6
- [36] Minseop Kwak, Jiuhn Song, and Seungryoung Kim. Geconerf: Few-shot neural radiance fields via geometric consistency. In *International Conference on Machine Learning, ICML 2023, 23-29 July 2023, Honolulu, Hawaii, USA*, pages 18023–18036. PMLR, 2023. 1, 2, 4, 5
- [37] Jiahe Li, Jiawei Zhang, Xiao Bai, Jin Zheng, Xin Ning, Jun Zhou, and Lin Gu. Dngaussian: Optimizing sparse-view 3d gaussian radiance fields with global-local depth normalization. In *IEEE/CVF Conference on Computer Vision and Pattern Recognition, CVPR 2024, Seattle, WA, USA, June 16-22, 2024*, pages 20775–20785. IEEE, 2024. 1, 2, 7
- [38] Mengfei Li, Xiaoxiao Long, Yixun Liang, Weiyu Li, Yuan Liu, Peng Li, Xiaowei Chi, Xingqun Qi, Wei Xue, Wenhan Luo, Qifeng Liu, and Yike Guo. M-LRM: multi-view large reconstruction model. *CoRR*, abs/2406.07648, 2024. 3
- [39] Zhan Li, Zhang Chen, Zhong Li, and Yi Xu. Spacetime gaussian feature splatting for real-time dynamic view synthesis. In *IEEE/CVF Conference on Computer Vision and*

- Pattern Recognition, CVPR 2024, Seattle, WA, USA, June 16-22, 2024*, pages 8508–8520. IEEE, 2024. 2
- [40] Chen-Hsuan Lin, Wei-Chiu Ma, Antonio Torralba, and Simon Lucey. BARF: bundle-adjusting neural radiance fields. In *2021 IEEE/CVF International Conference on Computer Vision, ICCV 2021, Montreal, QC, Canada, October 10-17, 2021*, pages 5721–5731. IEEE, 2021. 3
- [41] Fangfu Liu, Wenqiang Sun, Hanyang Wang, Yikai Wang, Haowen Sun, Junliang Ye, Jun Zhang, and Yueqi Duan. Reconx: Reconstruct any scene from sparse views with video diffusion model. *CoRR*, abs/2408.16767, 2024. 3, 5
- [42] Lingjie Liu, Jiatao Gu, Kyaw Zaw Lin, Tat-Seng Chua, and Christian Theobalt. Neural sparse voxel fields. In *Advances in Neural Information Processing Systems 33: Annual Conference on Neural Information Processing Systems 2020, NeurIPS 2020, December 6-12, 2020, virtual*, 2020. 2
- [43] Xi Liu, Chaoyi Zhou, and Siyu Huang. 3dgs-enhancer: Enhancing unbounded 3d gaussian splatting with view-consistent 2d diffusion priors. *arXiv preprint arXiv:2410.16266*, 2024. 3
- [44] Andreas Meuleman, Yu-Lun Liu, Chen Gao, Jia-Bin Huang, Changil Kim, Min H. Kim, and Johannes Kopf. Progressively optimized local radiance fields for robust view synthesis. In *IEEE/CVF Conference on Computer Vision and Pattern Recognition, CVPR 2023, Vancouver, BC, Canada, June 17-24, 2023*, pages 16539–16548. IEEE, 2023. 3
- [45] Ben Mildenhall, Pratul P. Srinivasan, Matthew Tancik, Jonathan T. Barron, Ravi Ramamoorthi, and Ren Ng. Nerf: Representing scenes as neural radiance fields for view synthesis. In *Computer Vision - ECCV 2020 - 16th European Conference, Glasgow, UK, August 23-28, 2020, Proceedings, Part I*, pages 405–421. Springer, 2020. 1, 2
- [46] Thomas Müller, Alex Evans, Christoph Schied, and Alexander Keller. Instant neural graphics primitives with a multiresolution hash encoding. *ACM Trans. Graph.*, 41(4):102:1–102:15, 2022. 2
- [47] Frank Plastria. The weiszfeld algorithm: Proof, amendments, and extensions. 2011. 3
- [48] Ben Poole, Ajay Jain, Jonathan T. Barron, and Ben Mildenhall. Dreamfusion: Text-to-3d using 2d diffusion. In *The Eleventh International Conference on Learning Representations, ICLR 2023, Kigali, Rwanda, May 1-5, 2023*. OpenReview.net, 2023. 2
- [49] Alec Radford, Jong Wook Kim, Chris Hallacy, Aditya Ramesh, Gabriel Goh, Sandhini Agarwal, Girish Sastry, Amanda Askell, Pamela Mishkin, Jack Clark, Gretchen Krueger, and Ilya Sutskever. Learning transferable visual models from natural language supervision. In *Proceedings of the 38th International Conference on Machine Learning, ICML 2021, 18-24 July 2021, Virtual Event*, pages 8748–8763. PMLR, 2021. 2
- [50] Christian Reiser, Songyou Peng, Yiyi Liao, and Andreas Geiger. Kilonerf: Speeding up neural radiance fields with thousands of tiny mlps. In *2021 IEEE/CVF International Conference on Computer Vision, ICCV 2021, Montreal, QC, Canada, October 10-17, 2021*, pages 14315–14325. IEEE, 2021. 2
- [51] Christian Reiser, Stephan J. Garbin, Pratul P. Srinivasan, Dor Verbin, Richard Szeliski, Ben Mildenhall, Jonathan T. Barron, Peter Hedman, and Andreas Geiger. Binary opacity grids: Capturing fine geometric detail for mesh-based view synthesis. *ACM Trans. Graph.*, 43(4):149:1–149:14, 2024. 2
- [52] Jeremy Reizenstein, Roman Shapovalov, Philipp Henzler, Luca Sbordone, Patrick Labatut, and David Novotny. Common objects in 3d: Large-scale learning and evaluation of real-life 3d category reconstruction. In *International Conference on Computer Vision*, 2021. 6
- [53] Robin Rombach, Andreas Blattmann, Dominik Lorenz, Patrick Esser, and Björn Ommer. High-resolution image synthesis with latent diffusion models. In *IEEE/CVF Conference on Computer Vision and Pattern Recognition, CVPR 2022, New Orleans, LA, USA, June 18-24, 2022*, pages 10674–10685. IEEE, 2022. 2, 5
- [54] Johannes Lutz Schönberger and Jan-Michael Frahm. Structure-from-motion revisited. In *Conference on Computer Vision and Pattern Recognition (CVPR)*, 2016. 3, 7
- [55] Steven M. Seitz and Charles R. Dyer. Photorealistic scene reconstruction by voxel coloring. In *1997 Conference on Computer Vision and Pattern Recognition (CVPR '97), June 17-19, 1997, San Juan, Puerto Rico*, pages 1067–1073. IEEE Computer Society, 1997. 2
- [56] Cheng Sun, Min Sun, and Hwann-Tzong Chen. Direct voxel grid optimization: Super-fast convergence for radiance fields reconstruction. In *IEEE/CVF Conference on Computer Vision and Pattern Recognition, CVPR 2022, New Orleans, LA, USA, June 18-24, 2022*, pages 5449–5459. IEEE, 2022. 2
- [57] Cheng Sun, Min Sun, and Hwann-Tzong Chen. Direct voxel grid optimization: Super-fast convergence for radiance fields reconstruction. In *IEEE/CVF Conference on Computer Vision and Pattern Recognition, CVPR 2022, New Orleans, LA, USA, June 18-24, 2022*, pages 5449–5459. IEEE, 2022. 1, 2, 6, 7
- [58] Jiaming Sun, Zehong Shen, Yuang Wang, Hujun Bao, and Xiaowei Zhou. Loftr: Detector-free local feature matching with transformers. In *IEEE Conference on Computer Vision and Pattern Recognition, CVPR 2021, virtual, June 19-25, 2021*, pages 8922–8931. Computer Vision Foundation / IEEE, 2021. 3
- [59] Wei Sun, Xiaosong Zhang, Fang Wan, Yanzhao Zhou, Yuan Li, Qixiang Ye, and Jianbin Jiao. Correspondence-guided sfm-free 3d gaussian splatting for NVS. *CoRR*, abs/2408.08723, 2024. 2, 3
- [60] Roman Suvorov, Elizaveta Logacheva, Anton Mashikhin, Anastasia Remizova, Arsenii Ashukha, Aleksei Silvestrov, Naejin Kong, Harshith Goka, Kiwoong Park, and Victor Lempitsky. Resolution-robust large mask inpainting with fourier convolutions. In *IEEE/CVF Winter Conference on Applications of Computer Vision, WACV 2022, Waikoloa, HI, USA, January 3-8, 2022*, pages 3172–3182. IEEE, 2022. 5
- [61] Matthew Tancik, Ethan Weber, Evonne Ng, Ruilong Li, Brent Yi, Terrance Wang, Alexander Kristoffersen, Jake Austin, Kamyar Salehi, Abhik Ahuja, David McAllister, Justin Kerr, and Angjoo Kanazawa. Nerfstudio: A modular framework for neural radiance field development.

- In *ACM SIGGRAPH 2023 Conference Proceedings, SIGGRAPH 2023, Los Angeles, CA, USA, August 6-10, 2023*, pages 72:1–72:12. ACM, 2023. 2
- [62] Jiaxiang Tang, Jiawei Ren, Hang Zhou, Ziwei Liu, and Gang Zeng. Dreamgaussian: Generative gaussian splatting for efficient 3d content creation. In *The Twelfth International Conference on Learning Representations, ICLR 2024, Vienna, Austria, May 7-11, 2024*. OpenReview.net, 2024. 2
- [63] Shinji Umeyama. Least-squares estimation of transformation parameters between two point patterns. *IEEE Trans. Pattern Anal. Mach. Intell.*, 13(4):376–380, 1991. 7
- [64] Chen Wang, Xian Wu, Yuan-Chen Guo, Song-Hai Zhang, Yu-Wing Tai, and Shi-Min Hu. Nerf-sr: High quality neural radiance fields using supersampling. In *MM '22: The 30th ACM International Conference on Multimedia, Lisboa, Portugal, October 10 - 14, 2022*, pages 6445–6454. ACM, 2022. 2
- [65] Guihang Wang, Xuejin Chen, and Si Chen. Cut-and-fold: Automatic 3d modeling from a single image. In *2013 IEEE International Conference on Multimedia and Expo Workshops, Chengdu, China, July 14-18, 2014*, pages 1–6. IEEE Computer Society, 2014. 2
- [66] Guangcong Wang, Zhaoxi Chen, Chen Change Loy, and Ziwei Liu. Sparsenerf: Distilling depth ranking for few-shot novel view synthesis. In *IEEE/CVF International Conference on Computer Vision, ICCV 2023, Paris, France, October 1-6, 2023*, pages 9031–9042. IEEE, 2023. 2
- [67] Jiuniu Wang, Hangjie Yuan, Dayou Chen, Yingya Zhang, Xiang Wang, and Shiwei Zhang. Modelscope text-to-video technical report. *CoRR*, abs/2308.06571, 2023. 5
- [68] Peng Wang, Lingjie Liu, Yuan Liu, Christian Theobalt, Taku Komura, and Wenping Wang. Neus: Learning neural implicit surfaces by volume rendering for multi-view reconstruction. In *Advances in Neural Information Processing Systems 34: Annual Conference on Neural Information Processing Systems 2021, NeurIPS 2021, December 6-14, 2021, virtual*, pages 27171–27183, 2021. 2
- [69] Shuzhe Wang, Vincent Leroy, Yohann Cabon, Boris Chidlovskii, and Jérôme Revaud. Dust3r: Geometric 3d vision made easy. In *IEEE/CVF Conference on Computer Vision and Pattern Recognition, CVPR 2024, Seattle, WA, USA, June 16-22, 2024*, pages 20697–20709. IEEE, 2024. 3, 4
- [70] Yunlong Wang, Fei Liu, Zilei Wang, Guangqi Hou, Zhenan Sun, and Tieniu Tan. End-to-end view synthesis for light field imaging with pseudo 4dcnn. In *Computer Vision - ECCV 2018 - 15th European Conference, Munich, Germany, September 8-14, 2018, Proceedings, Part II*, pages 340–355. Springer, 2018. 2
- [71] Zhou Wang, Alan C. Bovik, Hamid R. Sheikh, and Eero P. Simoncelli. Image quality assessment: from error visibility to structural similarity. *IEEE Trans. Image Process.*, 13(4): 600–612, 2004. 7
- [72] Zirui Wang, Shangzhe Wu, Weidi Xie, Min Chen, and Victor Adrian Prisacariu. Nerf-: Neural radiance fields without known camera parameters. *CoRR*, abs/2102.07064, 2021. 1, 3, 7
- [73] Zhengyi Wang, Yikai Wang, Yifei Chen, Chendong Xiang, Shuo Chen, Dajiang Yu, Chongxuan Li, Hang Su, and Jun Zhu. CRM: single image to 3d textured mesh with convolutional reconstruction model. *CoRR*, abs/2403.05034, 2024. 3
- [74] Rundi Wu, Ben Mildenhall, Philipp Henzler, Keunhong Park, Ruiqi Gao, Daniel Watson, Pratul P. Srinivasan, Dor Verbin, Jonathan T. Barron, Ben Poole, and Aleksander Holynski. Reconfusion: 3d reconstruction with diffusion priors. In *IEEE/CVF Conference on Computer Vision and Pattern Recognition, CVPR 2024, Seattle, WA, USA, June 16-22, 2024*, pages 21551–21561. IEEE, 2024. 1, 3, 5
- [75] Jinbo Xing, Menghan Xia, Yong Zhang, Hao Chen, Wangbo Yu, Hanyuan Liu, Gongye Liu, Xintao Wang, Ying Shan, and Tien-Tsin Wong. Dynamicrafter: Animating open-domain images with video diffusion priors. In *Computer Vision - ECCV 2024 - 18th European Conference, Milan, Italy, September 29-October 4, 2024, Proceedings, Part XLVI*, pages 399–417. Springer, 2024. 5
- [76] Haolin Xiong, Sairisheek Muttukuru, Rishi Upadhyay, Pradyumna Chari, and Achuta Kadambi. Sparsegs: Real-time 360° sparse view synthesis using gaussian splatting. *CoRR*, abs/2312.00206, 2023. 2, 4, 5
- [77] Dejia Xu, Yifan Jiang, Peihao Wang, Zhiwen Fan, Humphrey Shi, and Zhangyang Wang. Sinnerf: Training neural radiance fields on complex scenes from a single image. In *Computer Vision - ECCV 2022 - 17th European Conference, Tel Aviv, Israel, October 23-27, 2022, Proceedings, Part XXII*, pages 736–753. Springer, 2022. 1, 2, 5
- [78] Zhiwen Yan, Weng Fei Low, Yu Chen, and Gim Hee Lee. Multi-scale 3d gaussian splatting for anti-aliased rendering. In *IEEE/CVF Conference on Computer Vision and Pattern Recognition, CVPR 2024, Seattle, WA, USA, June 16-22, 2024*, pages 20923–20931. IEEE, 2024. 2
- [79] Lihe Yang, Bingyi Kang, Zilong Huang, Zhen Zhao, Xiaogang Xu, Jiashi Feng, and Hengshuang Zhao. Depth anything V2. *CoRR*, abs/2406.09414, 2024. 4
- [80] Botao Ye, Sifei Liu, Haofei Xu, Xueting Li, Marc Pollefeys, Ming-Hsuan Yang, and Songyou Peng. No pose, no problem: Surprisingly simple 3d gaussian splats from sparse unposed images. *arXiv preprint arXiv:2410.24207*, 2024. 3
- [81] Vickie Ye, Ruilong Li, Justin Kerr, Matias Turkulainen, Brent Yi, Zhuoyang Pan, Otto Seiskari, Jianbo Ye, Jeffrey Hu, Matthew Tancik, and Angjoo Kanazawa. gsplat: An open-source library for Gaussian splatting. *arXiv preprint arXiv:2409.06765*, 2024. 7
- [82] Ruihong Yin, Vladimir Yugay, Yue Li, Sezer Karaoglu, and Theo Gevers. Fewviews: Gaussian splatting with few view matching and multi-stage training. *arXiv preprint arXiv:2411.02229*, 2024. 1, 2, 4
- [83] Hanyang Yu, Xiaoxiao Long, and Ping Tan. Lm-gaussian: Boost sparse-view 3d gaussian splatting with large model priors. *CoRR*, abs/2409.03456, 2024. 3, 5
- [84] Wangbo Yu, Jinbo Xing, Li Yuan, Wenbo Hu, Xiaoyu Li, Zhipeng Huang, Xiangjun Gao, Tien-Tsin Wong, Ying Shan, and Yonghong Tian. Viewrafter: Taming video diffusion models for high-fidelity novel view synthesis. *CoRR*, abs/2409.02048, 2024. 3, 5

- [85] Zehao Yu, Anpei Chen, Binbin Huang, Torsten Sattler, and Andreas Geiger. Mip-splatting: Alias-free 3d gaussian splatting. In *IEEE/CVF Conference on Computer Vision and Pattern Recognition, CVPR 2024, Seattle, WA, USA, June 16-22, 2024*, pages 19447–19456. IEEE, 2024. [1](#), [2](#)
- [86] Hongjia Zhai, Xiyu Zhang, Boming Zhao, Hai Li, Yijia He, Zhaopeng Cui, Hujun Bao, and Guofeng Zhang. Splatloc: 3d gaussian splatting-based visual localization for augmented reality. *CoRR*, abs/2409.14067, 2024. [1](#)
- [87] Kai Zhang, Gernot Riegler, Noah Snavely, and Vladlen Koltun. Nerf++: Analyzing and improving neural radiance fields. *CoRR*, abs/2010.07492, 2020. [2](#)
- [88] Kai Zhang, Sai Bi, Hao Tan, Yuanbo Xiangli, Nanxuan Zhao, Kalyan Sunkavalli, and Zexiang Xu. GS-LRM: large reconstruction model for 3d gaussian splatting. In *Computer Vision - ECCV 2024 - 18th European Conference, Milan, Italy, September 29-October 4, 2024, Proceedings, Part XXII*, pages 1–19. Springer, 2024. [3](#)
- [89] Richard Zhang, Phillip Isola, Alexei A. Efros, Eli Shechtman, and Oliver Wang. The unreasonable effectiveness of deep features as a perceptual metric. In *2018 IEEE Conference on Computer Vision and Pattern Recognition, CVPR 2018, Salt Lake City, UT, USA, June 18-22, 2018*, pages 586–595. Computer Vision Foundation / IEEE Computer Society, 2018. [7](#)
- [90] Qingtian Zhu, Zizhuang Wei, Zhongtian Zheng, Yifan Zhan, Zhuyu Yao, Jiawang Zhang, Kejian Wu, and Yinqiang Zheng. Rpbg: Towards robust neural point-based graphics in the wild. In *Computer Vision - ECCV 2024*, 2024. [2](#)
- [91] Zehao Zhu, Zhiwen Fan, Yifan Jiang, and Zhangyang Wang. FSGS: real-time few-shot view synthesis using gaussian splatting. In *Computer Vision - ECCV 2024 - 18th European Conference, Milan, Italy, September 29-October 4, 2024, Proceedings, Part XXXIX*, pages 145–163. Springer, 2024. [1](#), [2](#), [5](#), [7](#)